 ISSN: 2229-3159

RESEARCH ARTICLE

MANY-BODY THEORY CALCULATIONS OF POSITRON BINDING TO NEGATIVE IONS

J.A. LUDLOW* AND G.F. GRIBAKIN

Department of Applied Mathematics and Theoretical Physics, Queen's University Belfast, Belfast BT7 1NN, Northern Ireland, UK

Abstract: A many-body theory approach developed by the authors [*Phys. Rev. A* **70** 032720 (2004)] is applied to positron bound states and annihilation rates in atomic systems. Within the formalism, full account of virtual positronium (Ps) formation is made by summing the electron-positron ladder diagram series, thus enabling the theory to include all important many-body correlation effects in the positron problem. Numerical calculations have been performed for positron bound states with the hydrogen and halogen negative ions, also known as Ps hydride and Ps halides. The Ps binding energies of 1.118, 2.718, 2.245, 1.873 and 1.393 eV and annihilation rates of 2.544, 2.482, 1.984, 1.913 and 1.809 ns^{-1}, have been obtained for PsH, PsF, PsCl, PsBr and PsI, respectively.

PACS Numbers: 36.10.Dr, 71.60.+z, 78.70.Bj, 82.30.Gg.

1. INTRODUCTION

A many-body theory approach developed by the authors (Gribakin and Ludlow 2004) takes into account all main correlation effects in positron-atom interactions. These are: polarization of the atomic system by the positron, virtual positronium formation and enhancement of the electron-positron contact density due to their Coulomb attraction. The first two effects are crucial for an accurate description of positron-atom scattering and the third one is very important for calculating positron annihilation rates. In this paper we apply our method to calculate the energies and annihilation rates for positron bound states with the hydrogen and halogen negative ions.

Positron bound states can have a strong effect on positron annihilation with matter. For example, positron bound states with molecules give rise to vibrational Feshbach resonances, which leads to a strong enhancement of the positron annihilation rates in many polyatomic molecular gases (Gribakin 2000, 2001, Gilbert et al. 2002, Gribakin et al. 2010). Nevertheless, the question of positron binding with neutral atoms or molecules has been answered in the affirmative only recently, and the ubiquity of such states is only becoming clear now (Dzuba et al. 1995, Ryzhikh and Mitroy 1997, Mitroy et al. 2001, 2002, Danielson 2009). On the other hand, it has been known for many decades that positrons bind to negative ions. Beyond the electron-positron bound state, or positronium (Ps), the simplest atomic system capable of binding the positron is the negative hydrogen ion (Ore 1951). The binding energy, annihilation rate and structure of the resulting compound, positronium hydride (PsH) have now been calculated to very high precision, e.g., by variational methods (Frolov et al. 1997). The information available for heavier negative ions with many valence electrons is not nearly as accurate (see Schrader and Moxom 2001 for a useful review). Positronium halides have received most of the attention, with some calculations dating back fifty years; see, e.g., the Hartree-Fock calculations of Simons (1953) and Cade and Farazdel (1977), quantum Monte-Carlo work by Schrader et al (1992a, 1993), and more recent configuration interaction results (Saito 1995, 2005, Saito and Hidao 1998, Miura and Saito 2003).

At first glance, the physics of positron binding to negative ions is much simpler than that of positron binding to neutrals. The driving force here is the Coulomb attraction between the particles. However, in contrast with atoms, the electron binding energy in a negative ion (i.e.,

* *Present Address:* Department of Physics, Auburn University, Auburn, AL 36849, USA.
E-mail: ludlow@physics.auburn.edu and *g.gribakin@qub.ac.uk*

the electron affinity, EA) is always smaller than the binding energy of Ps, $|E_{1s}| \approx 6.8$ eV. This means that the lowest dissociation threshold in the positron-anion system is that of the neutral atom and Ps, so that the positron bound to a negative ion may still escape by Ps emission. Hence, for the system to be truly bound, its energy should lie below the Ps-atom threshold, and the positron energy in the bound state, ε_0, must satisfy:

$$|\varepsilon_0| > |E_{1s}| - \mathrm{EA}. \qquad \ldots (1)$$

This situation is similar to positron binding to atoms with ionization potentials smaller than 6.8 eV. The structure of these bound states is characterized by a large "Ps cluster" component (Mitroy et al. 2002).

The proximity of the Ps threshold in anions means that to yield accurate binding energies, the method used must account for virtual Ps formation. The positron also polarizes the electron cloud, inducing an attractive polarization potential. It has the form $-\alpha e^2/2r^4$ at large positron-target separations r, where α is the dipole polarizability of the target The method should thus be capable of describing many-electron correlation effects. The halogen negative ions have np^6 valence configurations, and are similar to noble-gas atoms. Here many-body theory may have an advantage over few-body methods (Dzuba et al. 1996).

The many-body theory approach developed by the authors (Gribakin and Ludlow 2004), employs B-spline basis sets. This enables the sum of the electron-positron ladder diagram sequence, or vertex function, to be found exactly. This vertex function accounts for virtual Ps formation. It is incorporated into the diagrams for the positron correlation potential and correlation corrections to the electron-positron annihilation vertex. To ensure convergence with respect to the maximum orbital angular momentum of the intermediate electron and positron states in the diagrams, $l_{\max}$, we use extrapolation. It is based on the known asymptotic behaviour of the energies and annihilation rates as functions of $l_{\max}$ (Gribakin and Ludlow 2002).

In Gribakin and Ludlow (2004) the theory has been successfully applied to positron scattering and annihilation on hydrogen below the Ps formation threshold, where the present formalism is exact. This theory is now extended to treat the more difficult problem of positron interaction with multielectron atomic negative ions. We test the method for H^-, and consider the halogen negative ions F^-, Cl^-, Br^- and I^-. Note that a conventional notation for the positron bound with a negative ion A^- is PsA, rather than e^+A^-, hence one has PsH, PsF, etc. (Schrader 1998).

2. CALCULATION OF POSITRON BINDING USING DYSON'S EQUATION

The many-body theory method for positron bound states is similar to that developed for electron-atom binding in negative ions (Chernysheva et al. 1988, Johnson et al. 1989, Gribakin et al. 1990, Dzuba et al. 1994), and used for positron-atom bound states by Dzuba et al. (1995).

The Green function of the positron interacting with a many-electron system ("target") satisfies the Dyson equation (see, e.g., Migdal 1967),

$$\left(E - \hat{H}_0\right) G_E(\mathbf{r}, \mathbf{r}') - \int \Sigma_E(\mathbf{r}, \mathbf{r}'') G_E(\mathbf{r}'', \mathbf{r}')\, \mathrm{d}\mathbf{r}'' = \delta(\mathbf{r} - \mathbf{r}'), \qquad \ldots (2)$$

where $\hat{H}_0$ is the zeroth-order positron Hamiltonian, and Σ_E is the *self-energy*. A convenient choice of $\hat{H}_0$ is that of the positron moving in the field of the Hartree-Fock (HF) target ground state. The self-energy then describes the correlation interaction between the positron and the target beyond the static-field HF approximation (Bell and Squires 1959). It can be calculated by means of the many-body diagrammatic expansion in powers of the electron-positron and electron-electron Coulomb interactions (see below).

If the positron is capable of binding to the system, i.e., the target has a positive positron affinity PA, the positron Green function $G_E(\mathbf{r}, \mathbf{r}')$ has a pole at $E = \varepsilon_0 \equiv -\mathrm{PA}$,

$$G_E(\mathbf{r}, \mathbf{r}') \underset{E \to \varepsilon_0}{\simeq} \frac{\psi_0(\mathbf{r})\, \psi_0^*(\mathbf{r}')}{E - \varepsilon_0}. \qquad \ldots (3)$$

Here $\psi_0(\mathbf{r})$ is the quasiparticle wavefunction which describes the bound-state positron. It is equal to the projection of the total ground-state wavefunction of the positron and N electrons, $\Psi_0(\mathbf{r}_1, \ldots, \mathbf{r}_N, \mathbf{r})$, onto the target ground-state wavefunction, $\Phi_0(\mathbf{r}_1, \ldots, \mathbf{r}_N)$,

$$\psi_0(\mathbf{r}) = \int \Phi_0^*(\mathbf{r}_1, \ldots, \mathbf{r}_N)\, \Psi_0(\mathbf{r}_1, \ldots, \mathbf{r}_N, \mathbf{r})\, d\mathbf{r}_1 \ldots \mathrm{d}\mathbf{r}_N. \qquad \ldots (4)$$

The normalization integral for $\psi_0(\mathbf{r})$,

$$a = \int |\psi_0(\mathbf{r})|^2\, \mathrm{d}\mathbf{r} < 1, \qquad \ldots (5)$$

can be interpreted as the probability that the electronic subsystem of the positron-target complex remains in its ground state.

The magnitude of a quantifies the extent to which the structure of the complex is that of the positron bound to the anion, e^+A^-, as opposed to that of the Ps atom orbiting the neutral atom. Such separation is a feature of the "heuristic wavefunction model" (Mitroy et al. 2002). If the former component dominates the wavefunction, the value of a is expected to be close to unity. If, on the other hand, the wavefunction contains a large "Ps cluster" component, the value of a will be notably smaller.

By taking the limit $E \to \varepsilon_0$ in Eq. (2), one obtains the Dyson equation for the quasiparticle wavefunction $\psi_0(\mathbf{r})$ ("Dyson orbital") and the bound-state energy ε_0,

$$\hat{H}_0 \psi_0(\mathbf{r}) + \int \Sigma_{\varepsilon_0}(\mathbf{r}, \mathbf{r}') \psi_0(\mathbf{r}') \, d\mathbf{r}' = \varepsilon_0 \psi_0(\mathbf{r}). \quad ...(6)$$

This equation is analogous to the standard Schrödinger eigenvalue problem, except that the correlation potential Σ depends on the energy.

The eigenstates $\varphi_\varepsilon(\mathbf{r})$ of the Hamiltonian $\hat{H}_0$,

$$\hat{H}_0 \varphi_\varepsilon(\mathbf{r}) = \varepsilon \varphi_\varepsilon(\mathbf{r}), \quad ... (7)$$

are characterized by their energies ε and the orbital angular momentum l, implicit in this notation. They form a complete single-particle positron basis set. For negative ions the spectrum of $\hat{H}_0$ consists of both discrete (Rydberg) and continuum states. This set can be used to expand the quasiparticle bound-state wavefunction:

$$\psi_0(\mathbf{r}) = \sum_\varepsilon C_\varepsilon \varphi_\varepsilon(\mathbf{r}), \quad ... (8)$$

and cast the Dyson equation, Eq. (6) in the matrix form:

$$\varepsilon C_\varepsilon + \sum_{\varepsilon'} \langle \varepsilon | \Sigma_{\varepsilon_0} | \varepsilon' \rangle C_{\varepsilon'} = \varepsilon_0 C_\varepsilon, \quad ... (9)$$

where the sums in Eqs (8) and (9) include the positive-energy continuum, as well as the discrete negative-energy states, and

$$\langle \varepsilon | \Sigma_E | \varepsilon' \rangle = \int \varphi^*_\varepsilon(\mathbf{r}) \Sigma_E(\mathbf{r}, \mathbf{r}') \varphi_{\varepsilon'}(\mathbf{r}') \, d\mathbf{r} d\mathbf{r}'. \quad ... (10)$$

In practice the continuum is discretized by using a B-spline basis set (see below), and Eq. (9) becomes a matrix eigenvalue problem. Therefore, to find ε_0 and C_ε one simply needs to diagonalize the matrix:

$$\varepsilon \delta_{\varepsilon\varepsilon'} + \langle \varepsilon | \Sigma_E | \varepsilon' \rangle. \quad ... (11)$$

Its lowest eigenvalue $\varepsilon_0(E)$ depends on the energy E at which Σ_E is calculated, and the diagonalization must be repeated several times until self-consistency is achieved: $\varepsilon_0(E) = E$. Knowing the dependence of the eigenvalue on E allows one to determine the normalization integral, Eq. (5), via the relation (Migdal 1967),

$$a = \left(1 - \left. \frac{\partial \varepsilon_0(E)}{\partial E} \right|_{E = \varepsilon_0} \right)^{-1}. \quad ... (12)$$

Note that owing to the spherical symmetry of the target, the states φ_ε and ψ_0 have definite orbital angular momenta. To find the bound positron ground state it is sufficient to calculate the self-energy matrix (10) for the s-wave positron only.

The accuracy of the binding energy obtained from the Dyson equation depends upon the accuracy to which the self-energy has been determined. As mentioned in the Introduction, polarization of the target and virtual Ps formation are the two most important effects that need to be accounted for. The effect of target polarization is described in the leading order by the 2nd-order diagram $\Sigma^{(2)}$, Fig. 1 (a). Following Gribakin and Ludlow (2004), the Ps formation contribution $\Sigma^{(\Gamma)}$ shown in Fig. 1 (b), is obtained by summing the electron-positron ladder diagram series to all orders, Fig. 2. This procedure amounts to calculation of the electron-positron vertex function Γ shown by the shaded block. Analytical expressions for the diagrams can be found in Gribakin and Ludlow (2004).

For hydrogen, the self-energy is given exactly by the two diagrams in Fig. 1, $\Sigma = \Sigma^{(2)} + \Sigma^{(\Gamma)}$, provided the intermediate electron and positron states are calculated in the field of the bare nucleus (Gribakin and Ludlow 2004). For multi-electron targets one may also consider higher-order corrections not included in the virtual Ps contribution, Fig. 1 (b). In the present calculation a set of 3rd-order diagrams shown in Fig. 3 will be included. Diagrams (a), (b), (c) and (d) represent corrections to the 2nd-order polarization diagram, of the type described by the random-phase approximation with exchange (RPAE, Amusia et al. 1975). They account for the electron-hole interaction and screening of the positron Coulomb field, and correct the value of the dipole polarizability α of the target. Diagram (e) accounts for

the positron-hole repulsion. The contribution of the diagrams in Fig. 3 is denoted collectively by $\Sigma^{(3)}$. Calculation of these diagrams will allow us to gauge the importance of these corrections, and even to include effectively higher-order diagrams (see below).

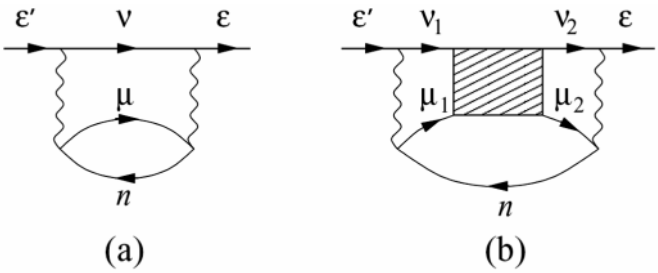

Fig. 1: Main contributions to the positron self-energy. Diagram (a) describes the effect of polarization in the lowest, second order, $\Sigma^{(2)}$; diagram (b) accounts for virtual Ps formation, $\Sigma^{(\Gamma)}$. Top lines in the diagrams describe the positron. Other lines with the arrows to the right are excited electron states, and to the left – holes, i.e. electron states occupied in the target ground state. Wavy lines are the Coulomb interactions. Summation over the intermediate positron, electron and hole states is carried out.

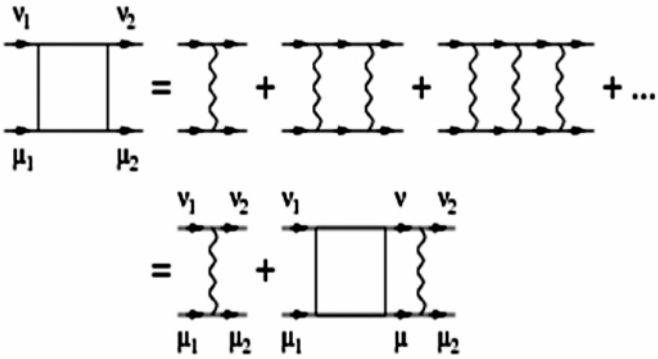

Fig. 2: Electron-positron ladder diagram series and its sum, the vertex function Γ (shaded block). Comparison between the left- and right-hand sides of the diagrammatic equation shows that Γ can be found by solving a linear matrix equation.

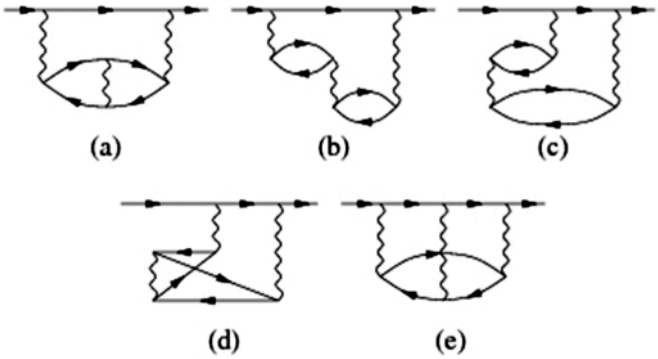

Fig. 3: Third-order contributions to the positron self-energy, $\Sigma^{(3)}$. Mirror images of the diagrams (c) and (d) are also included. The top line describes the positron.

Of course, any many-body theory calculation can at best include only dominant classes of diagrams, leaving out an infinite number of other higher-order diagrams. For example, the diagram in Fig. 4 has the effect of screening the positron-electron interaction accompanying virtual Ps formation in $\Sigma^{(\Gamma)}$, Fig. 1 (b).

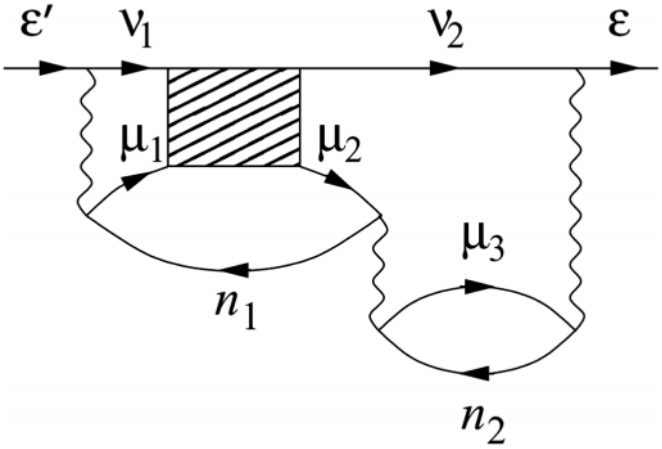

Fig. 4: Screening correction to the virtual Ps contribution $\Sigma^{(\Gamma)}$.

The number of diagrams increases rapidly as one moves to higher orders. The effort required to evaluate these diagrams becomes prohibitive relative to their small contribution. It would therefore be useful to find a simple method to estimate the contribution of the higher-order diagrams. This will allow us to take into account the effect of electron screening beyond the corrections shown in Fig. 3.

A useful quantity for estimating the size of a contribution to the self-energy Σ is a dimensionless measure of its "strength" (Dzuba et al. 1994),

$$g_E(\Sigma) = \int G^{(0)}(\mathbf{r}', \mathbf{r})\, \Sigma_E(\mathbf{r}, \mathbf{r}')\, d\mathbf{r} d\mathbf{r}'$$

$$= -\sum_{\nu} \frac{\langle \varepsilon_\nu | \Sigma_E | \varepsilon_\nu \rangle}{\varepsilon_\nu} \qquad \ldots (14)$$

where $G^{(0)}$ is the 0th-order positron Green function calculated at $E = 0$. Let:

$$S_E = \frac{g_E\left(\Sigma^{(3)}\right)}{g_E\left(\Sigma^{(2)}\right)} \qquad \ldots (15)$$

be the ratio of the strength of the sum of the 3rd-order polarization diagrams (Fig. 3) to the strength of the 2nd-order polarization diagram. This quantity S_E can then be used to estimate higher-order contributions to $\Sigma^{(\Gamma)}$.

As a check, we test that the binding energy obtained using $\Sigma^{(2+3)} = \Sigma^{(2)} + \Sigma^{(3)}$ is close to that obtained with $\Sigma^{(2)}$ multiplied by $1 + S_E$, i.e., using

$$(1 + S_E)\,\Sigma^{(2)} \equiv \Sigma^{(2+3')}. \qquad \ldots (16)$$

An estimate of the *total* self-energy corrected for the screening effects in the lowest order can then be obtained as:

$$\left(1 + S_E\right)\left[\Sigma^{(2)} + \Sigma^{(\Gamma)}\right]. \qquad \ldots (17)$$

As we will see in Section 4, the relative effect of screening is negative, $S_E < 0$, which means that screening reduces the magnitude of the self-energy. Similar higher-order terms in the self-energy expansion will alternate in sign. Thus, for example, a diagram such as that shown in Fig. 5, will tend to compensate the lowest-order screening correction in Fig. 4.

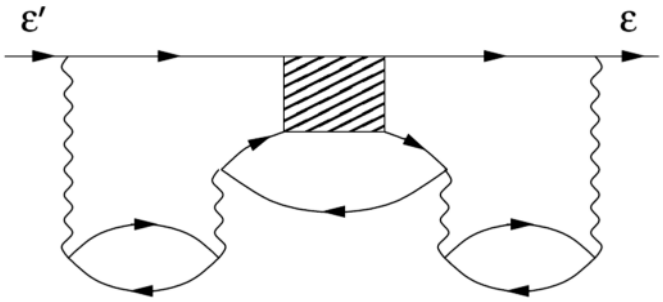

Fig. 5: Higher-order screening correction to the virtual Ps contribution $\Sigma^{(\Gamma)}$, cf. Fig. 4.

Assuming that the sequence of screening corrections behaves like a geometric series, its effect can approximately be taken into account by using the *screened* self-energy, which we denote $\Sigma^{(\mathrm{scr})}$:

$$\Sigma^{(\mathrm{scr})} = \frac{1}{1 - S_E}\left[\Sigma^{(2)} + \Sigma^{(\Gamma)}\right]. \qquad \ldots (18)$$

We expect that this approximation should yield our best prediction for the binding energy.

3. CALCULATION OF THE POSITRON ANNIHILATION RATE IN THE BOUND STATE

The spin-averaged positron annihilation rate Γ_a in the bound state can be expressed in terms of the average contact electron-positron density ρ_{ep} (see, e.g., Berestetskii et al. 1982)

$$\Gamma_a = \pi r_0^2 c \rho_{ep}, \qquad \ldots (19)$$

where r_0 is the classical radius of the electron, c is the speed of light, and ρ_{ep} is given by the integral,

$$\rho_{ep} = \sum_{i=1}^{N} \int \left|\Psi_0\left(\mathbf{r}_1, \mathbf{r}_2, \ldots, \mathbf{r}_N, \mathbf{r}\right)\right|^2 \times \delta\left(\mathbf{r} - \mathbf{r}_i\right) d\mathbf{r}_1 \ldots d\mathbf{r}_N d\mathbf{r} \qquad \ldots (20)$$

where $\Psi_0(\mathbf{r}_1, \mathbf{r}_2, \ldots, \mathbf{r}_N, \mathbf{r})$ is the full $(N + 1)$-particle bound-state wavefunction of the N electron coordinates $\mathbf{r}_i$ and positron coordinate $\mathbf{r}$.

Figure 6 shows a series of diagrams that would constitute a complete set of annihilation diagrams for a one-electron system (Gribakin and Ludlow 2004). Here ε represents the positron bound-state Dyson orbital $\psi_0(\mathbf{r})$ normalized as per Eq. (5).

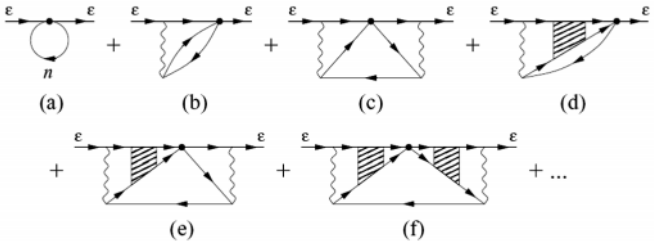

Fig. 6: Many-body theory expansion for the contact electron-positron density. The solid circle in the diagrams is the delta-function annihilation vertex, cf. Eq. (20). Diagrams (b), (d) and (e) are multiplied by two to account for their mirror images.

Diagram (a) in Fig. 6 is the overlap of the positron and HF electron densities. It represents the independent-particle approximation to the annihilation vertex with the contact density:

$$\rho_{ep}^{(0)} = \sum_{n=1}^{N} \int \left|\phi_n(\mathbf{r})\right|^2 \left|\psi_0(\mathbf{r})\right|^2 d\mathbf{r} \qquad \ldots (21)$$

where $\phi_n(r)$ is the HF orbital of hole n. The first-order correction, diagram (b), can be thought of as the analogue of $\Sigma^{(2)}$, and will be denoted by $\rho_{ep}^{(1)}$. The diagrams with the vertex function Γ, e.g., (d) in Fig. 6, are particularly important in the calculation of ρ_{ep}, as the annihilation takes place at a point, and is strongly enhanced by the Coulomb attraction in the annihilating electron-positron pair.

The diagrams shown in Fig. 6, represent a basic set of contributions with a single hole line, which one needs to consider to obtain a reliable answer. We will denote

the corresponding density as $\rho_{ep}^{(0)} + \rho_{ep}^{(\Delta)}$, $\rho_{ep}^{(\Delta)}$ representing a correction to the zeroth-order contact density. Similar to the self-energy diagrams in Fig. 1, they represent the exact answer for the positron-hydrogen system, provided the electron and positron intermediate states are calculated in the field of the bare nucleus (Gribakin and Ludlow 2004). For complex many-electron systems it may be necessary to account for the effects of electron screening when calculating ρ_{ep}. A series of RPA-type annihilation diagrams is therefore also calculated, see Fig. 7.

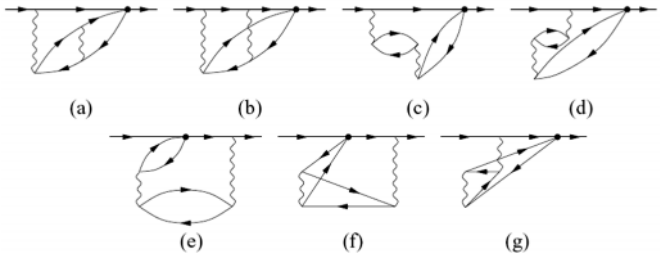

Fig. 7: Annihilation diagrams with two Coulomb interactions, including those of RPA-type, $\rho_{ep}^{(2)}$. The top line describes the positron. All the diagrams have equal mirror images.

Similarly, screening corrections to the annihilation diagrams containing the Γ block can also be considered, as shown in Fig. 8.

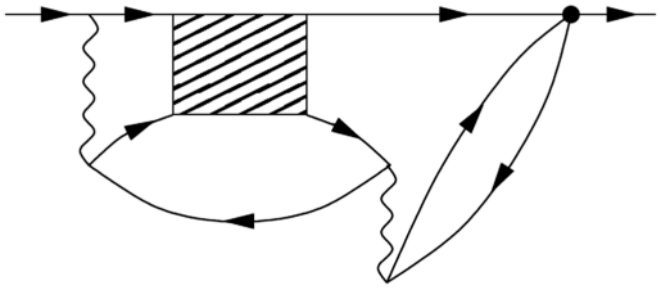

Fig. 8: Screening correction to the annihilation diagram containing the vertex function Γ.

The diagrams shown in Fig. 7, $\rho_{ep}^{(2)}$, can be thought of as next-order corrections to $\rho_{ep}^{(1)}$, diagram (b) in Fig. 6. By evaluating the ratio:

$$C = \rho_{ep}^{(2)} / \rho_{ep}^{(1)}, \qquad \ldots (22)$$

an estimate can be made of the total contact density ρ_{ep} that includes higher-order corrections in a manner similar to the self-energy [cf. Eq. (18)],

$$\rho_{ep} = \rho_{ep}^{(0)} + \frac{1}{1-C}\rho_{ep}^{(\Delta)}. \qquad \ldots (23)$$

4. NUMERICAL IMPLEMENTATION

The Hartree-Fock ground state of the negative ions is first found. The frozen-core HF Hamiltonian for an electron or a positron (with and without exchange, respectively) is then diagonalized in a B-spline basis (Sapirstein et al. 1996). The corresponding eigenvectors provide bases of single-particle electron and positron states, cf. Eq. (7). The spectrum of these states for the electron includes the negative-energy ground-state orbitals (hole states) and positive-energy excited states spanning the electron continuum, see, e.g., Fig. 6 in Gribakin and Ludlow (2004). The positron basis contains a number of negative-energy Rydberg states augmented by the discretized positive energy positron "continuum".

The effective spanning of the continuum is achieved by using an exponential radial knot sequence for the B-splines. For H^-, the first 23 eigenstates generated from a set of 60 splines of order 9 were used, with a box size of R = 30 au. For the other systems, namely F^-, Cl^-, Br^- and I^-, the first 20 states from a set of 40 splines of order 6 were used with R = 30 au. Only the outermost s and p subshells were included when calculating the self-energy and annihilation diagrams. More strongly bound inner-shell electrons are only weakly perturbed by the positron. Their contribution to the correlation potential and annihilation vertex is relatively small, and has been neglected.

The diagrammatic contributions to the self-energy and contact density described in Sections 2 and 3, are calculated by direct summation over the intermediate electron and positron states, and the vertex function is found by solving a linear matrix equation. The use of B-spline bases ensures quick convergence with respect to the number of states with a particular angular momentum l included in the calculation. In addition, the convergence with respect to the maximum orbital angular momentum included in the calculation, $l_{\max}$, also needs to be considered. This is done by extrapolation through the use of the asymptotic formulae (Gribakin and Ludlow 2002),

$$\varepsilon_0 = \varepsilon_0^{(l_{\max})} - \frac{A}{(l_{\max}+1/2)^3}, \qquad \ldots (24)$$

and

$$\rho_{ep} = \rho_{ep}^{(l_{\max})} + \frac{B}{(l_{\max}+1/2)}, \qquad \ldots (25)$$

where $\varepsilon_0^{(l_{\max})}$ and $\rho_{ep}^{(l_{\max})}$ are the bound-state energy and contact density obtained in a calculation for a given $l_{\max}$, and A and B are constants. While the derivation of

Eqs (24) and (25) is based on perturbation theory (Gribakin and Ludlow 2002), this asymptotic behaviour is confirmed by nonperturbative many-body-theory calculations (Gribakin and Ludlow 2004), and by configuration-interaction calculations of positron binding and annihilation in atoms (Mitroy and Bromley 2006). The constants A and B are found numerically and have different values for each system studied.

5. RESULTS

5.1. Details of Calculations for PsCl

In this section, a detailed examination of the results for PsCl will be presented. This should illustrate how the final results for the other systems were arrived at.

The positron radial wavefunctions for PsCl obtained by solving the Dyson equation using the *ab initio* self-energy $\Sigma^{(2+\Gamma+3)}$ and the screened self-energy $\Sigma^{(scr)}$ are compared to the HF positron wavefunction in Fig. 9. The inclusion of the attractive correlation potential results in lower energies of the positron bound states, and hence, more compact wavefunctions. Otherwise the two Dyson orbitals are very similar to each other.

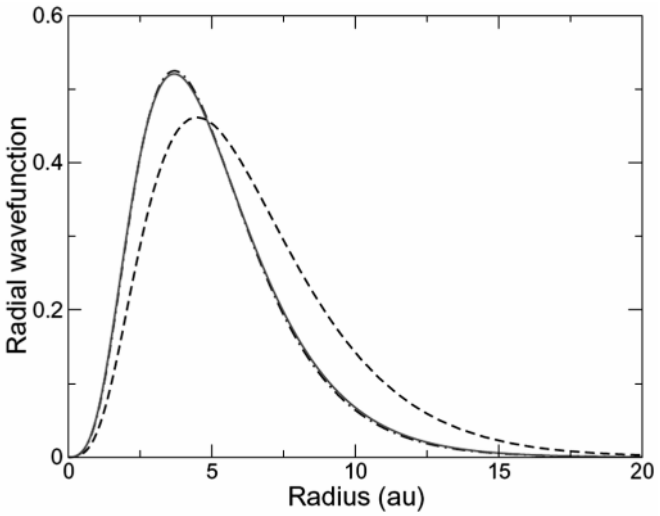

Fig. 9: Radial positron wavefunction in PsCl: ---, Hartree–Fock; — · —, Dyson orbital calculated using the self-energy $\Sigma^{(2+\Gamma+3)}$; —, Dyson orbital obtained with $\Sigma^{(scr)}$. The HF and Dyson orbitals on the graph are normalized to unity.

When solving the Dyson equation, the self-energy and the bound-state energy ε_0 were calculated for a number of maximum orbital angular momenta, e.g., l_{max} = 7 – 10, and then the asymptotic behaviour (24) was used to find the result for $l_{max} \to \infty$. This procedure is illustrated for PsCl in Fig. 10. Extrapolation from l_{max} = 10 to infinity increases the binding energy by about 0.5%.

Before the contact density ρ_{ep} can be determined, the positron Dyson orbital must be correctly normalized via Eq. (12). This is achieved by calculating the self-energy for a number of energies E and finding the lowest eigenvalue of the matrix (11) at these energies, giving $\varepsilon_0(E)$. This is repeated to self-consistency, $E = \varepsilon_0(E)$, and the gradient $\partial\varepsilon_0(E)/\partial E$ is found at this point. This is illustrated for PsCl in Fig. 11.

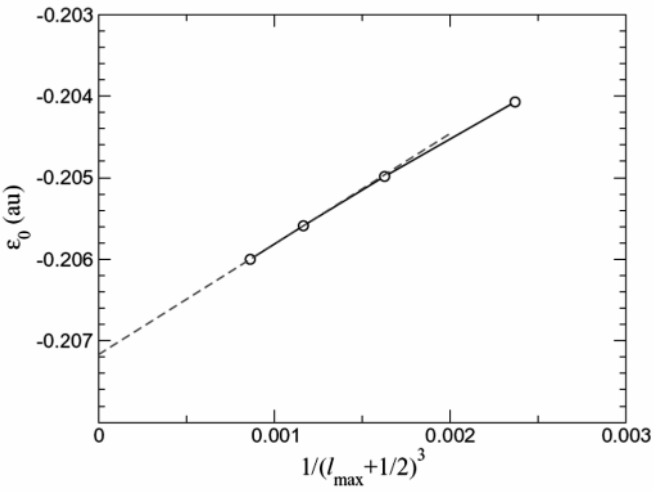

Fig. 10: Convergence of the binding energy for PsCl as a function of l_{max}. Open circles connected by a solid line to guide the eye, show the energies ε_0 calculated using $\Sigma^{(2+\Gamma+3)}$ at E = –0.207 au for l_{max} = 7–10; dashed line shows extrapolation.

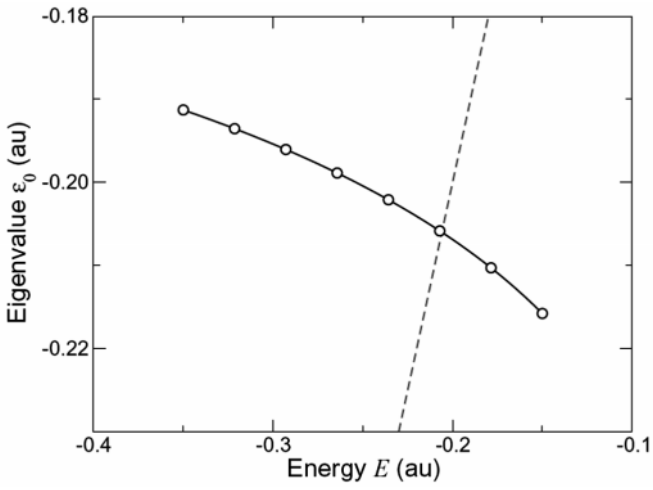

Fig. 11: Open circles connected by the solid line show the positron energy $\varepsilon_0(E)$ for PsCl obtained from the Dyson equation with $\Sigma^{(2+\Gamma+3)}$, as a function of the energy at which the self-energy was calculated; dashed line is $\varepsilon_0 = E$. The intersection of the two lines, $\varepsilon_0(E) = E$, gives the binding energy. The gradient of $\varepsilon_0(E)$ at this point is used to calculate the normalization constant a from Eq. (5).

According to Eq. (25), the electron-positron contact density ρ_{ep} converges much more slowly than the energy, and extrapolation with respect to l_{max} is much more

important here. This is illustrated for PsCl in Fig. 12. Extrapolation beyond l_{max} = 10 increases the contact density, and hence, the annihilation rate, by about 30%.

The calculations are performed for a number of approximations to the self-energy. This enables us to determine the relative magnitude of various diagrams, and helps to clarify which physical effects are important to include so as to obtain an accurate binding energy. The positron energies obtained for PsCl using different approximations are given in Table 1.

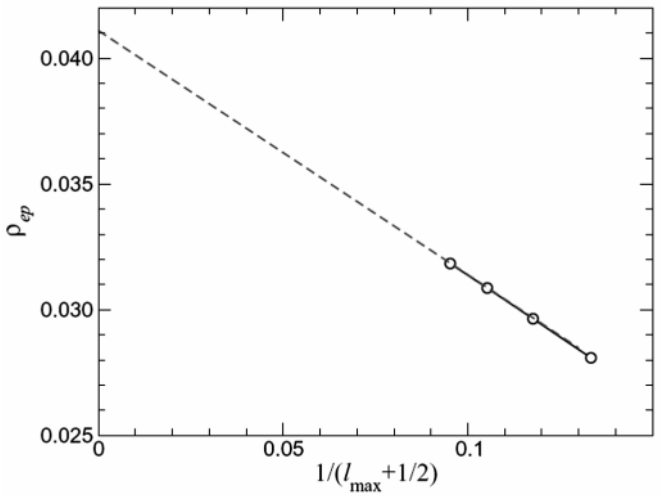

Fig. 12: Convergence of the electron-positron contact density ρ_{ep} for PsCl as a function of l_{max}. Open circles connected by a solid line to guide the eye, show values of $\rho_{ep}^{(0)} + \rho_{ep}^{(\Delta)} + \rho_{ep}^{(2)}$ obtained for l_{max} = 7–10 in the calculation using $\Sigma^{(2+\Gamma+3)}$; dashed line shows extrapolation.

Table 1
Positron bound-state energies ε_0 (in au) for Cl^- obtained using various approximations to the correlation potential

HF	$\Sigma^{(2)}$	$\Sigma^{(2+\Gamma)}$	$\Sigma^{(2+3)}$	$\Sigma^{(2+\Gamma+3)}$	$\Sigma^{(2+\Sigma+3)}$	$\Sigma^{(scr)}$
−0.1419	−0.1855	−0.2276	−0.1663	−0.2072	−0.1641	−0.1998

In the HF approximation, the energy of the lowest s wave positron state is −0.1419 au. The Ps binding energy (BE) is determined from the positron affinity PA = $|\varepsilon_0|$ using Eq. (26), which gives BE = 0.672 eV. This value is in agreement with the HF results of Cade et al. (1977). Therefore, PsCl is bound even in the static HF approximation. However, the self-energy is essential in determining an accurate binding energy. The second-order polarization diagram $\Sigma^{(2)}$ increases the binding energy, and the inclusion of the virtual Ps formation contribution $\Sigma^{(\Gamma)}$ increases it even further. When we add the 3rd-order corrections $\Sigma^{(3)}$ to $\Sigma^{(2)}$, the binding reduces noticeably. This means that screening of the Coulomb interaction is important. In particular, the positron binding energy of 0.2276 au, obtained with $\Sigma^{(2+\Gamma)}$, becomes equal to 0.2072 au when the total self-energy $\Sigma^{(2+\Sigma+3)}$ is used.

However, this calculation neglects the effect of screening on the virtual Ps-formation contribution $\Sigma^{(\Gamma)}$. Evaluating the magnitude of screening via Eq. (15) we obtain S_E = −0.45. When the effect of screening on $\Sigma^{(2)}$ is included via the factor 1 + S_E, as per Eq. (16), add closing parenthesis the corresponding result (labelled $\Sigma^{(2+3')}$ is very close to that obtained with $\Sigma^{(2+3)}$ (see Table 1). The application of approximation (18), denoted $\Sigma^{(scr)}$, gives our best estimate of the positron binding energy, 0.1998 au, corresponding to a Ps binding energy of 2.245 eV. This value is only slightly below the completely *ab initio* value of 2.437 eV obtained using $\Sigma^{(2+\Gamma+3)}$.

The contact densities calculated using the Dyson orbitals obtained with $\Sigma^{(2+\Gamma+3)}$ and $\Sigma^{(scr)}$ are quite close, as are the energies and wavefunctions. We show the breakdown of the contributions to ρ_{ep} in Table 2. To appreciate the scale of densities involved, it is useful to remember that the contact density of ground state Ps is ρ_{ep}(Ps) = 1/8π ≈ 0.0398 au. Note that although $\Sigma^{(2+\Gamma+3)}$ gives a slightly larger binding energy and a more compact positron wavefunction than $\Sigma^{(scr)}$, the densities obtained in the former approximation are lower. This is due to a smaller normalization constant *a*, which results from a somewhat stronger energy dependence of $\Sigma^{(2+\Gamma+3)}$.

Table 2
Breakdown of contributions to the electron-positron contact density in PsCl (in au)

Approx.	$\rho_{ep}^{(0)}$	$\rho_{ep}^{(1)}$	$\rho_{ep}^{(0)} + \rho_{ep}^{(\Delta)}$	$\rho_{ep}^{(0)}$	*total*	ρ_{ep}, *Eq. (23)*
$\Sigma^{(2+\Gamma+3)}$	0.00841	0.00931	0.04263	−0.00155	0.04108	–
$\Sigma^{(scr)}$	0.00872	0.00964	0.04444	−0.00162	0.04281	0.03929

The zeroth-order diagram, $\rho_{ep}^{(0)}$ gives only about 20% of the total density, with $\rho_{ep}^{(1)}$ giving another 20% and the rest coming from higher order diagrams in $\rho_{ep}^{(\Delta)}$ (Fig. 6). As with the self-energy, the inclusion of screening effects ($\rho_{ep}^{(2)}$, Fig. 7) reduces the total. However, the effect of screening on the annihilation vertex is much smaller than that on the correlation potential, as indicated by the value of *C* = −0.17, Eq. (22). Physically, this is related to the fact that in the annihilation vertex corrections, small

electron-positron separations dominate. Finally, using Eq. (23) to account for the effect of screening on the diagrams in $\rho_{ep}^{(\Delta)}$ we obtain our best prediction for the contact density (last column in Table 2). This corresponds to the PsCl decay rate of 1.984 ns^{-1}, which is close to the spin-averaged decay rate of Ps, 2.01 ns^{-1}.

5.2 Results for PsH, PsF, PsCl, PsBr and PsI

The final results for PsH, PsF, PsCl, PsBr and PsI obtained with the correlation potential $\Sigma^{(2+\Gamma+3)}$ and density $\rho_{ep}^{(0)}+\rho_{ep}^{(\Delta)}+\rho_{ep}^{(2)}$, and $\Sigma^{(scr)}$ and screened densities from Eq. (23), are shown in Table 3. In all cases the positron is bound in the *s*-wave, all higher lying quasi-bound states being unstable against Ps emission. Note that the latter is true for the electron-spin-singlet states, as excited "unnatural parity" electron-spin-triplet Ps-atom bound states have been discovered recently for the hydrogen and the alkalis (Mitroy and Bromley 2007, Mitroy et al. 2007).

The positron binding energy is highest in PsH. This is a consequence of the small size of the hydrogen atom, and the small value of its electron affinity, which makes for strong electron-positron correlation effects. Beyond PsH the binding energy decreases along the halogen sequence, mostly due to a stronger positron repulsion from the positively-charged atomic cores in heavier systems.

Values of the normalization parameter *a* in Table 3 give some insight into the structure of these compounds. PsH has the smallest value of *a* and its structure therefore has a large component that describes Ps bound to the neutral atom ("Ps cluster"), the small electron affinity of H playing a role in this. PsF has the largest value of *a* and its structure can best be described as a positron bound to F^-. Generally, all of the compounds considered have large values of *a*. This indicates that a positron bound to the negative ion is the dominant component of the structure. This is a consequence of the stable noble-gas-like structure of the halogen negative ions. In contrast, positron bound states with the weakly-bound alkali negative ions have a distinct Ps-atom character (Mitroy et al. 2002).

It is interesting to compare the positron wavefunctions obtained from the Dyson equation for H^- and the halogen anions. In Fig. 13, the wavefunctions obtained with the self-energy $\Sigma^{(2+\Gamma+3)}$ are shown. The shape of the positron wavefunction is determined by a balance between the Coulomb and correlation-potential attraction at large separations, and the Coulomb repulsion from the nucleus at smaller radii. The positron wavefunctions for PsH and PsF are quite similar. This feature reflects the high positron binding energy to the H^- and F^- ions, and the fact that the corresponding atoms have the smallest radii. As the positron binding energy decreases, the positron wavefunction relaxes outwards. This feature is seen as one moves along the halogen sequence. One can also observe the increasing "expulsion" of the positron from the atomic core region, caused by the Coulomb repulsion from the nucleus.

Table 3
Positron binding energies, normalization constants and contact densities for PsH and positronium halides

Compound	ε_0^a *au*	a^a	ρ_{ep}^a	ε_0^b *au*	a^b	ρ_{ep}^b
PsH	−0.27619	0.714	0.05231	−0.26338	0.748	0.05037
PsF	−0.22778	0.950	0.04790	−0.22489	0.958	0.04913
PsCl	−0.20718	0.875	0.04108	−0.19975	0.894	0.03929
PsBr	−0.20373	0.834	0.03910	−0.19523	0.868	0.03788
PsI	−0.19805	0.794	0.03707	−0.18878	0.835	0.03582

[a] Dyson equation solved using $\Sigma^{(2+\Gamma+3)}$, density $\rho_{ep}=\rho_{ep}^{(0)}+\rho_{ep}^{(\Delta)}+\rho_{ep}^{(2)}$.

[b] Dyson equation solved using $\Sigma^{(scr)}$, density ρ_{ep} from Eq. (23).

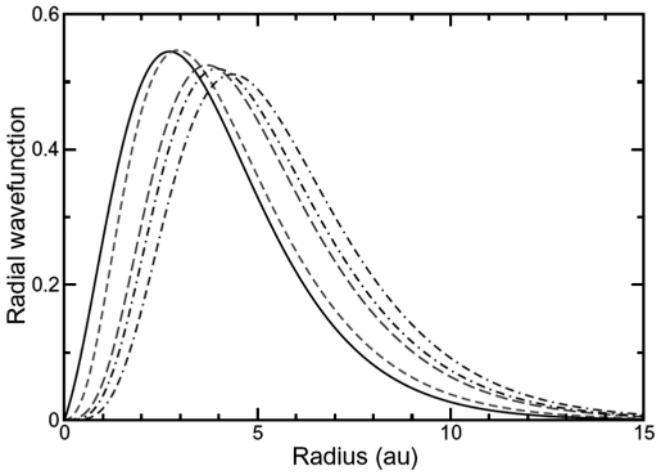

Fig. 13: Comparison of the radial Dyson orbitals obtained with $\Sigma^{(2+\Gamma+3)}$: solid, PsH; dashed, PsF; long-dashed, PsCl; dot-dashed, PsBr; dot-double-dashed, PsI. For the purpose of comparison, all orbitals are normalized to unity.

5.3 Comparison with other Theoretical Results

The positron binding energies can be converted to Ps binding energies via the simple relation,

$$\mathrm{BE}\,(\mathrm{Ps}A) = \mathrm{EA}\,(A) + \mathrm{PA}\,(A^-) + E_{1s}\,(\mathrm{Ps}), \qquad \ldots (26)$$

where BE (PsA) is the binding energy of a Ps atom to a generic atom denoted by A, EA (A) is the electron affinity of the atom, PA (A^-) is the positron affinity of the negative ion and E_{1s} (Ps) = –6.8028 eV is the spin-averaged energy of Ps. For the electron affinities needed, the values of 0.7542 eV for H, 3.4012 eV for F, 3.6127 eV for Cl, 3.3636 eV for Br and 3.0590 eV for I, have been used (Andersen et al. 1999).

Annihilation rates Γ_a in units of ns^{-1} are obtained by dividing the contact density ρ_{ep} by the conversion factor 10^9 s/($\pi r_0^2 c$) = 0.0198 ns × au. The final Ps binding energies and positron annihilation rates are shown in Table 4, and compared with other calculations and experiment.

Table 4
Ps binding energies and positron annihilation rates for PsH and positronium halides compared with other calculations and experiment

Compound	*Present Results*		*Other Results*	
	Ps BE (eV)	Γ_a *(ns^{-1})*	*Ps BE (eV)*	Γ_a *(ns^{-1})*
PsH	1.118	2.544	1.066126[a] 1.1 ± 0.2[i]	2.4361[a]
PsF	2.718	2.482	2.806[b] 2.70[c] 2.24[d] 1.98 ± 0.17[g] 2.838[f] 2.9 ± 0.5[j]	2.019[b] 1.98[c]
PsCl	2.245	1.984	2.350[b] 1.91 ± 0.16[e] 1.62[d] 2.0 ± 0.5[j]	1.504[b]
PsBr	1.873	1.913	2.061[b] 1.14 ± 0.11[g] 1.25[h]	1.371[b]
PsI	1.393	1.809	1.714[b] 0.56[h]	1.254[b]

Theory: [a]Frolov et al. 1997, [b]Saito 2005, [c]Miura and Saito 2003, [d]Saito 1995, [e]Schrader et al. 1992a, [f]Bressanini et al. 1998, [g]Schrader et al. 1993, [h]Saito et al. 1998.

Experiment: [i]Schrader et al. 1992b, [j]Tao et al. 1969.

For PsH very accurate variational calculations are available (Frolov et al. 1997). Our many-body theory calculations are in good agreement with these results, and both the Ps binding energy and positron annihilation rate are accurate to within 5%. Because of the small electron affinity of hydrogen, PsH is more difficult for many-body theory to treat than larger, more tightly bound systems with many valence electrons. The results for the heavier systems should therefore be of similar or possibly even of greater accuracy than the results for PsH.

For PsF a few theoretical calculations are available, the present Ps binding energy and positron annihilation rate agreeing most closely with multi-reference configuration-interaction calculations (Miura and Saito 2003, Saito 2005). The Ps binding energy is also close to a diffusion Monte-Carlo calculation by Bressanini et al. (1998).

The present Ps binding energies for PsCl, PsBr and PsI are greater than those obtained using a second-order variational perturbation method (Saito et al. 1995, 1998) and Monte-Carlo calculations (Schrader et al. 1992a, 1993). Our values are in better agreement with, although consistently smaller than, multi-reference configuration-interaction calculations by Saito (2005). The positron annihilation rates from the present calculation and that of Saito (2005) are in reasonable agreement, although our values are consistently higher.

5.4 Comparison with Experiment

For PsH, a direct experimental measurement of the Ps binding energy (Schrader et al. 1992b) is available. In this experiment, the reaction $e^+ + CH_4 \rightarrow CH_3^+ + PsH$ was studied by detecting the CH_3^+ ions. From the experimentally determined threshold energy for CH_3^+ production and the various bond energies, a value of 1.1 ± 0.2 eV was found for the PsH binding energy. This value is in excellent agreement with theory, though much less precise.

So far, there have been no direct experimental measurements of the Ps binding energy for the halogens, however estimates of the Ps binding energy for PsF and PsCl have been made (Tao et al. 1969), see Table 4. The PsCl binding energy was estimated by studying positron annihilation in Cl_2 and Ar-Cl_2 gas mixtures. The appearance of a shoulder in the positron annihilation lifetime spectrum was attributed to the reaction, $Ps + Cl_2 \rightarrow PsCl + Cl$. From a knowledge of the energy at which this shoulder begins and the Cl_2 dissociation energy, a binding energy of about 2.0 eV was estimated for PsCl. The estimate of the PsF binding energy was obtained from the observation that when a hydrogen atom in benzene is replaced by fluorine, the fraction of positrons annihilating with the longest lifetime, as ortho-positronium, was reduced from 40 to 27%. This reduction was assumed to be due to the reaction, $C_6H_5F + Ps \rightarrow$

$PsF + C_6H_5$. From a knowledge of the threshold energy and the relevant dissociation energies, a binding energy of about 2.9 eV was estimated for PsF. The present results support these early estimates. This can be in part due to underestimation of the contribution of high orbital angular momenta by the extrapolation procedure used by Saito (Mitroy and Bromley 2005).

6. CONCLUDING REMARKS

Traditionally, many-body theory has had more success in treating purely electronic systems (Chernysheva et al. 1988, Dzuba and Gribakin 1994), than systems that contain a positron. In particular, earlier many-body theory calculations relied on very simple (Amusia et al. 1976) or approximate (Dzuba et al. 1995, 1996) treatments of the virtual Ps formation contribution to the correlation potential. However, it is now clear that many-body theory is capable of giving positron and Ps binding energies and positron annihilation rates that are accurate to within a few percent for many-electron systems.

The calculated binding energies and annihilation rates for positronium halides should serve as a useful reference for other theoretical calculations and future experiments. We have also performed an extended analysis of various contributions to the correlation potential and contact density, especially of the role of screening. This will be helpful for the problem of positron scattering and annihilation on noble-gas atoms. In the future it will be important to calculate explicitly the contribution of the RPA-type screening diagrams and also to move to a fully relativistic framework, particularly for heavy atoms and ions.

ACKNOWLEDGMENTS

The work of JL has been supported by DEL.

REFERENCES

[1] Amusia M. Ya and Cherepkov N.A., 1975, "Case Studies in Atomic Physics", **5,** 47.

[2] Amusia M. Ya, Cherepkov N.A., Chernysheva L.V. and Shapiro S.G., 1976, "J. Phys. B: At. Mol. Phys.", **9**, L531.

[3] Andersen T., Haugen H.K. and Hotop H., 1999, "J. Phys. Chem. Ref. Data". **28**, 1526.

[4] Bell J.S. and Squires E.J., 1959, "Phys. Rev. Lett.", **3,** 96.

[5] Berestetskii V.B., Lifshitz E.M. and Pitaevskii L.P., 1982, "Quantum Electrodynamics", (Butterworth-Heinemann, Oxford).

[6] Bressanini D., Mella M. and Morosi G., 1998, "J. Chem. Phys.", **108**, 4756.

[7] Cade P.E. and Farazdel A., 1977, "J. Chem. Phys.", **66**, 2598.

[8] Chernysheva L.V., Gribakin G.F., Ivanov V.K. and Kuchiev M. Yu, 1988, "J. Phys. B: At. Mol. Opt. Phys.", **21**, L419.

[9] Danielson J.R., Young J.A. and Surko C.M., 2009, "J. Phys. B: At. Mol. Opt. Phys.", **42**, 235203.

[10] Dzuba V.A. and Gribakin G.F., 1994, "Phys. Rev. A", **49**, 2483.

[11] Dzuba V.A., Flambaum V.V., Gribakin G.F. and King W.A., 1995, "Phys. Rev. A", **52**, 4541.

[12] Dzuba V.A., Flambaum V.V., Gribakin G.F. and King W.A., 1996, "J. Phys. B: At. Mol. Opt. Phys.", **29**, 3151.

[13] Frolov A.M. and Smith V.H. Jr., 1997, "Phys. Rev. A", **55**, 2662.

[14] Gilbert S.J., Barnes L.D., Sullivan J.P. and Surko C.M., 2002, "Phys. Rev. Lett.", **88**, 043201.

[15] Gribakin G.F., Gul'tsev B.V., Ivanov V.K. and Kuchiev M. Yu, 1990, "J. Phys. B: At. Mol. Opt. Phys.", **23**, 4505.

[16] Gribakin G.F., 2000, "Phys. Rev. A", **61**, 022720.

[17] Gribakin G.F., 2001, "New Directions in Antimatter Chemistry and Physics" ed CM Surko and FA Gianturco (The Netherlands: Kluwer Academic Publishers) pp. 413.

[18] Gribakin G.F. and Ludlow J., 2002, "J. Phys. B: At. Mol. Opt. Phys.", **35**, 339.

[19] Gribakin G.F., and Ludlow J., 2004, "Phys. Rev. A", **70**, 032720.

[20] Gribakin G.F., Young J.A. and Surko C.M., 2010, "Rev. Mod. Phys.", accepted for publication.

[21] Johnson W.R., Sapirstein J. and Blundell S.A., 1989, "J. Phys. B: At. Mol. Opt. Phys.", **22**, 2341.

[22] Migdal A.B., 1967, "Theory of Finite Fermi-Systems and Applications to Atomic Nuclei", (New York: Interscience).

[23] Mitroy J., Bromley M.W.J. and Ryzhikh G.G., 2001, "New Directions in Antimatter Chemistry and Physics", ed CM Surko and FA Gianturco (The Netherlands: Kluwer Academic Publishers) pp. 199.

[24] Mitroy J., Bromley M.W.J. and Ryzhikh G.G., 2002, "J. Phys. B: At. Mol. Opt. Phys.", **35**, R81.

[25] Mitroy J. and Bromley M.W.J., 2005, "J. Chem. Phys.", **123**, 017101.

[26] Mitroy J. and Bromley M.W.J., 2006, "Phys. Rev. A", **73**, 052712.

[27] Mitroy J. and Bromley M.W.J., 2007, "Phys. Rev. Lett.", **98**, 063401.

[28] Mitroy J., Bromley M.W.J. and Varga K., 2007, "Phys. Rev. A", **75**, 062505.

[29] Miura N. and Saito S.L., 2003, "Mol. Phys.", **101**, 143.

[30] Ore A., 1951, "Phys. Rev.", 83, 665.

[31] Ryzhikh G.G. and Mitroy J., 1997, "Phys. Rev. Lett.", **97**, 4123.

[32] Saito S.L., 1995, "Chem. Phys. Lett.", 245, **54**.

[33] Saito S.L. and Hidao S., 1998, "Chem. Phys. Lett.", **288**, 277.

[34] Saito S.L., 2005, "J. Chem. Phys.", **122**, 054302.

[35] Sapirstein J. and Johnson W.R., 1996, "J. Phys. B: At. Mol. Opt. Phys.", **29**, 5213.

[36] Schrader D.M., 1998, "Nucl. Instrum. Methods B", **143**, 209.

[37] Schrader D.M., Yoshida T. and Iguchi K., 1992a, "Phys. Rev. Lett.", **68**, 3281.

[38] Schrader D.M., Jacobsen F.M., Frandsen N.P. and Mikkelsen U., 1992b, "Phys. Rev. Lett.", **69**, 57.

[39] Schrader D.M., Yoshida T. and Iguchi K., 1993, "J. Chem. Phys.", **98**, 7185.

[40] Schrader D.M. and Moxom J., 2001, "New Directions in Antimatter Chemistry and Physics", ed CM Surko and FA Gianturco (The Netherlands: Kluwer Academic Publishers) pp. 263.

[41] Simons L., 1953, "Phys. Rev.", **90**, 165.

[42] Tao S.J. and Green J.W., 1969, "J. Phys. Chem.", **73**, 882.